Mon. Not. R. Astron. Soc. **000**, 1–17 (2013) Printed 13 February 2013 (MN LATEX style file v2.2)

The CASSOWARY spectroscopy survey: A new sample of gravitationally lensed galaxies in SDSS

Daniel P. Stark[1]†, Matthew Auger[2], Vasily Belokurov[2], Tucker Jones[3], Brant Robertson[1], Richard S. Ellis[4], David J. Sand[5], Alexei Moiseev[6], Will Eagle[2], Thomas Myers[2]

[1] *Steward Observatory, University of Arizona, 933 N Cherry Ave, Tucson, AZ, USA*
[2] *Institute of Astronomy, University of Cambridge, Madingley Road, Cambridge CB3 0HA, United Kingdom*
[3] *Department of Physics, University of California, Santa Barbara CA 93106, USA*
[4] *Department of Astronomy, California Institute of Technology, Pasadena, CA 91125 USA*
[5] *Department of Physics, Texas Tech University, Box 41051, Lubbock, TX 79409 USA*
[6] *Special Astrophysical Observatory, Nizhniy Arkhyz, Karachaevo-Cherkessiya, Russia*

Accepted ... ; Received ... ; in original form ...

ABSTRACT

Bright gravitationally lensed galaxies provide our most detailed view of galaxies at high redshift. The very brightest ($r < 21$) systems enable high spatial and spectral resolution measurements, offering unique constraints on the outflow energetics, metallicity gradients, and stellar populations in high redshift galaxies. Yet as a result of the small number of ultra-bright $z \simeq 2$ lensed systems with confirmed redshifts, most detailed spectroscopic studies have been limited in their scope. With the goal of increasing the number of bright lensed galaxies available for detailed follow-up, we have undertaken a spectroscopic campaign targeting wide separation ($\gtrsim 3''$) galaxy-galaxy lens candidates within the Sloan Digital Sky Survey (SDSS). Building on the earlier efforts of our CASSOWARY survey, we target a large sample of candidate galaxy-galaxy lens systems in SDSS using a well-established search algorithm which identifies blue arc-like structures situated around luminous red galaxies. In this paper, we present a new redshift catalog containing 25 lensed sources in SDSS confirmed through spectroscopic follow-up of candidate galaxy-galaxy lens systems. Included in this new sample are two of the brightest galaxies ($r = 19.6$ and 19.7) galaxies known at $z \simeq 2$, a low metallicity (12 + log (O/H) $\simeq 8.0$) extreme nebular line emitting galaxy at $z = 1.43$, and numerous systems for which detailed follow-up will be possible. The source redshifts span $0.9 < z < 2.5$ (median redshift of 1.9), and their optical magnitudes are in the range $19.6 \lesssim r \lesssim 22.3$. We present a brief source-by-source discussion of the spectroscopic properties extracted from our confirmatory spectra and discuss some initial science results. Preliminary lens modelling reveals average source magnifications of 5-10×. With more than 50 gravitationally-lensed $z \gtrsim 1$ galaxies now confirmed within SDSS, it will soon be possible for the first time to develop generalised conclusions from detailed spectroscopic studies of the brightest lensed systems at high redshift.

Key words: cosmology: observations - galaxies: evolution - galaxies: formation - galaxies: high-redshift

1 INTRODUCTION

Recent years have seen significant progress in the characterisation of star formation and feedback in high redshift galaxies. While much of these strides have stemmed from spectroscopic study of large samples of $z \simeq 2-4$ galaxies (e.g., Shapley 2011 for a recent review), strong gravitational lensing is now playing an increasingly important role. As typical galaxies are often too faint and too small to study individually in great detail, the magnification provided by strong gravitational lensing (often 10-30×) provides one of our only means of dissecting high redshift galaxies in great detail with current facilities.

Study of strongly-lensed gravitationally lensed galaxies helps high-redshift studies in two ways. First the flux amplification enables spectra of higher resolution and increased signal to noise, yielding unique constraints on the absorbing gas (Pettini et al. 2002, Quider et al. 2009, 2010, Dessauge-Zavadsky et al. 2010) and de-

⋆ E-mail: dpstark@email.arizona.edu
† Hubble Fellow.

tailed emission line studies of the ionised gas (e.g., Fosbury et al. 2003, Yuan et al. 2009, Hainline et al. 2009, Bian et al. 2010, Rigby et al. 2011, Richard et al. 2011, Wuyts et al. 2012, Brammer et al. 2012). Second, the increase in the apparent size of the lensed sources enables characterisation of the internal kinematics and metallicity gradients on scales as small as 100 parsec (e.g., Stark et al. 2008, Swinbank et al. 2009, Jones et al. 2010a, 2010b, 2012b).

A tremendous amount of physical information becomes accessible through analysis of the optical spectra of the brightest lensed galaxies. The wide array of interstellar absorption features that are detectable in the rest-frame UV of bright lensed galaxies enable abundances to be measured for numerous chemical elements. In a detailed study of MS 1512-cB58, one of the highest surface brightness lensed galaxies, Pettini et al. (2002) demonstrated that while the ISM is already heavily enriched with elements released in Type II supernovae, those elements (N and Fe-peak) produced on longer timescales (via intermediate mass stars and Type Ia supernovae) are significantly underabundant. These results provide a unique measure of the past star formation history, indicative of a picture whereby the bulk of metal enrichment has occurred in the past $\simeq 300$ Myr. Whether these abundance patterns vary with redshift, galaxy mass, or star formation rate remains unclear owing to the small sample of galaxies bright enough for such detailed analysis.

The absorption line measurements of ultra-bright lensed galaxies additionally provide our most complete picture of the kinematics and geometry of the interstellar gas. In the handful of lensed systems with detailed measurements, absorption is seen over a velocity range of 1000 km s^{-1} with respect to the stars. As expected, the bulk of the interstellar material in these systems is outflowing from the stars with typical speeds of 100-300 km s^{-1}. In the case of MS 1512-cB58, the rate at which mass is ejected in the outflow is shown to be comparable if not greater than rate at which gas is converted to stars (Pettini et al. 2000, 2002), consistent with recent inferences from the detection of a broadened component of Hα emission lines in unlensed $z \simeq 2$ galaxies from the SINS survey (Genzel et al. 2011, Newman et al. 2012). Further constraints on the outflow mass loading factor are of crucial importance to an understanding of how outflows regulate star formation and the chemical evolution of high redshift galaxies.

With the development of adaptive-optics assisted infrared integral field spectrographs on 8-10m telescopes, similarly unique insights are being achieved through measurement of the distribution of resolved properties within lensed galaxies at $z \simeq 2-3$. Most recently, resolved metallicity gradient measurements have been presented for five bright lensed galaxies (Jones et al. 2010b, 2012b; Yuan et al. 2011) with source plane resolution as fine as 300 pc. The current data point toward 2-3$\times$ steeper metallicity gradients at higher redshift, as expected in realistic models of inside-out growth (see Jones et al. 2012b); yet with the small existing samples of lensed galaxies with resolved metallicity measurements, significant uncertainties in the average gradient evolution remain.

Clearly the potential impact of lensing studies has been stunted by the small number of the brightest systems for which detailed analysis is possible. With only a handful of galaxies having absorption line measurements with adequate S/N and resolution, it is difficult to assess population averages of the mass loading factor and ISM chemical abundance patterns. Near-IR studies are more severely compromised, as many of the brightest systems happen to be located at redshifts which place their strong rest-optical emission lines behind sky lines. Larger samples of bright $z \simeq 2-3$ gravitationally-lensed galaxies are required to build upon the emerging framework. Fortunately, through a variety of imaging surveys ranging from the Sloan Digital Sky Survey (SDSS) to HST surveys of galaxy clusters (e.g., Ebeling et al. 2010), the number of bright lensed galaxies has rapidly increased in recent years.

Our group is one of several (see also e.g., Hennawi et al. 2008; Diehl et al. 2009; Kiester et al. 2010; Kubo et al. 2011; Bayliss et al. 2011a, 2011b; Bayliss 2012) that has actively exploited SDSS imaging for the purposes of locating galaxy galaxy lenses. As part of the Cambridge And Sloan Survey Of Wide ARcs in theskY; CASSOWARY), we have developed a search algorithm which targets multiple blue companions (or arcs) separated by $\gtrsim 3$ arcseconds from luminous red galaxies (Belokurov et al. 2009). The initial search (Belokurov et al. 2007) yielded discovery of SDSS J1148+1930 (the "Cosmic Horseshoe"), a highly-magnified $z = 2.38$ galaxy bright enough (r=19.5) for high resolution optical spectroscopy (Quider et al. 2009) and emission line mapping (Jones et al. 2012b), while subsequent exploration has yielded further candidates (e.g., Belokurov et al. 2009; Pettini et al. 2010; Christensen et al. 2010; Brewer et al. 2011). Typically the CASSOWARY systems correspond to lensing of $z \simeq 1-3$ star-forming galaxies by an early type galaxy and fainter group companions at $z \simeq 0.2$ - 0.7.

Yet in spite of this progress, there still remains nearly 50 bright candidate lensed systems in our photometric catalog (as well as catalogs of other teams, see Wen et al. 2011) without confirmed redshifts. Among those lacking confirmation are potentially some of the brightest gravitationally-lensed galaxies on the sky. To help build a more complete redshift database of the optically-brightest lensed galaxies in the SDSS footprint, we have undertaken a spectroscopic campaign (primarily with MMT, but also using Keck, Magellan, and LBT) to obtain redshifts for bright lensed candidates in our CASSOWARY catalog. Through these efforts, we present spectroscopic redshifts for 25 lensed CASSOWARY sources at $0.9 < z < 2.8$ detected within SDSS. As much of our focus is on the spatially-resolved and high spectral resolution study of high redshift galaxies (e.g., Stark et al. 2008; Quider et al. 2009, 2010; Jones et al. 2010a, 2010b, 2012b), we put significant effort into confirming those targets which are optimal for this study. Follow-up spectroscopy of the new CASSOWARY sample is under way and will be described in future papers.

The plan of the paper is as follows. In §2, we review the lens search algorithm and describe the observations undertaken for this program. In §3, we present the new redshift sample, providing a brief discussion of the spectroscopic properties of each new system. In §4, we describe preliminary lens models for select systems and comment on the typical star formation rates and stellar masses of the new CASSOWARY sample. In §5, we provide a more extended discussion of two lensed systems and describe some of the opportunities that will be made possible with the new sample.

Throughout the paper, we adopt a Λ-dominated, flat universe with $\Omega_\Lambda = 0.7$, $\Omega_M = 0.3$ and $\mathrm{H}_0 = 70\,\mathrm{h}_{70}\,\mathrm{km\,s^{-1}\,Mpc^{-1}}$. All magnitudes in this paper are quoted in the AB system (Oke et al. 1983).

2 LENS IDENTIFICATION AND OBSERVATIONS

We began a spectroscopic campaign of CASSOWARY candidate lensed galaxies in September of 2011. Below we review our SDSS lens search algorithm and then provide details of the instrumentation used on each of these facilities. An overview of the observations is provided in Table 1.

2.1 Lens search algorithm

The CASSOWARY survey (Belokurov et al. 2007, 2009) is designed to find gravitational lenses with angular Einstein diameters in excess of the size of the SDSS fibre ($\gtrsim 3''$). The motivation of the survey and the search procedure is described in detail in Belokurov et al. (2009). Here we provide a short summary.

Our lens search algorithm relies primarily on the SDSS photometric catalogues, rather than the actual images. The basic idea is to find massive elliptical galaxies surrounded by smaller objects with the spectral energy distributions (SEDs) suggestive of star-forming galaxies at $1 < z < 3$. The algorithm first identifies "seed" lenses by selecting massive Luminous Red Galaxies (LRGs) which we inspect for evidence of lensing. The LRG selection uses a modified version of the criteria presented in Eistenstein et al. (2001), allowing for slightly lower surface brightness, fainter apparent magnitude and slightly bluer colours. The SDSS photometric quality flags are used to cull the artefacts produced by severe blending and saturated stars.

In the second step, using the SDSS Neighbours list for each of our "seed lenses", we identified systems with more than 1 blue neighbour within 10-20$''$of the lens candidate. The exact criteria of how blue the arc candidates ought to be were tuned for different iterations of the search, but typically we require at least $(g-r)_S < 1$ or $(g-r)_S < (g-r)_L$ where "S" refers to the blue lensed source candidate and "L" corresponds to the red lens candidate.

The final step is to filter out false positives. There are several astrophysical phenomena other than strong gravitational lensing that could pass the first two filters. These include nearby spiral galaxies with prominent bulges, polar rings, and various configurations of minor mergers. We take advantage of the existing SDSS spectroscopy to filter out the majority of the nearby spirals. The polar rings and the mergers are picked out by visual inspection of the SDSS image cutouts. The final result of this procedure is a sample of $\gtrsim 100$ CASSOWARY gravitational lens candidates. We use this as the input catalog for our spectroscopic search described below.

2.2 MMT

Spectroscopic observations with MMT were conducted in longslit mode primarily with the Blue Channel Spectrograph. We used the 300 line grating of the Blue Channel Spectrograph, providing close to 5300 Å of spectral coverage. We typically used a central wavelength of 5500 Å with a UV-36 order blocking filter. We adopted a 1 arcsec slit width, providing a spectral resolution of 6.5 Å. Observations with the Blue Channel Spectrograph are optimal for confirming $z \gtrsim 2$ galaxies via detection of UV absorption lines.

In the redshift range $1.0 < z < 1.5$, it is far easier to confirm star-forming lensed galaxies through detection of [OII] emission in the red. We have thus also conducted observations with the MMT Red Channel Spectrograph. We used the 270 line/mm grating with a central wavelength in the range $\sim 7500 - 7900$ Å. As with our blue channel observations, we use a slit width of 1 arcsec, providing a spectral resolution of ~ 11 Å. The spectral coverage with this setting is 3705 Å, allowing detection of emission lines out to $\simeq 9300 - 9700$ Å, depending on the central wavelength. During our red channel runs, we occasionally targeted candidate $z \simeq 2$ lensed galaxies. In order to search for absorption from Si II λ1526, CIV λ1549, and Al II λ1671 in these $z \simeq 2$ sources, we used the 300 line/mm grating (with central wavelength of 5500 Å), providing useful coverage in the range 4230-7000 Å.

Exposure times varied from candidate to candidate depending on source brightness and conditions. We generally observed an individual galaxy for between 30 and 60 minutes. Specifics for each source are provided in Table 1. The conditions were typically clear but not always photometric. Seeing ranged from 0.″5-1.″5, but for most successful observations, the average seeing was $\lesssim 1''$.

Reduction of blue and red channel longslit spectra were conducted using standard routines. Wavelength calibration was performed with HeAr/Th arcs. Each spectrum was flux calibrated using spectral observations of standard stars.

2.3 Magellan

We obtained near-infrared spectra for several of the CASSOWARY systems using the Folded-port InfraRed Echellette (FIRE; Simcoe et al. 2010) on the 6.5 meter Magellan Baade Telescope. We used FIRE in echelle mode, delivering continuous spectral coverage between the z-band and K-band. The slit length of FIRE is 7 arcseconds. We adopted a slit width of 0.75 arc seconds, providing a resolving power of $\mathrm{R} = 4800$. The FIRE data were reduced using the custom FIREHOSE pipeline. Wavelength calibration was performed using OH sky lines. We have thus far secured emission lines for four of the galaxies in the sample presented in this paper. Details are listed in Table 1 and 2.

2.4 Keck

We used the DEIMOS spectrograph (Faber et al. 2003) on the Keck II telescope to confirm redshifts of several of our CASSOWARY candidates. These observations were typically conducted during runs focused on deep observations of $z \simeq 6$ galaxies. When conditions were not sufficient for such deep observations, we observed bright CASSOWARY targets. We used the 1200 line/mm grating which has a spectral resolution of $\simeq$ 1.1 Å. These observations were focused in the red, providing spectral coverage of 2630 Å in the wavelength range of 7000 to 10000 Å. Reduction was conducted using the standard spec2d DEIMOS pipeline. In total, we confirmed the redshifts of four lensed galaxies with DEIMOS. Further details are in Table 1.

2.5 LBT

We obtained near-infrared spectra for an arc toward SDSS J1958+5950, one of the brightest new CASSOWARY systems (Table 1), using the LUCI near-infrared spectrograph on the Large Binocular Telescope. We used the 200_H+K grating in two settings, one focused on the z and J-bands (0.95-1.40 μm) and a second targeting the the H and K-bands (1.50-2.30μm). We used a longslit with a width of 1.″0, providing a reasonably low spectral resolving power (R=940-1300). Data were reduced using an adapted version (see Bian et al. 2010 for details) of a near-IR spectral reduction pipeline (G. Becker 2012, private communication).

3 NEW SPECTROSCOPIC SAMPLE

Through the spectroscopic initiatives presented in §2, we have confirmed the redshifts for 25 bright gravitationally-lensed sources detected in SDSS. We also measure the redshifts of the lensing galaxy (or group) in systems where SDSS spectroscopy was not available. With the exception of a lensed arc and quasar recently reported in Dahle et al. 2012 and the $z = 0.909$ arc in Wuyts et al. (2012),

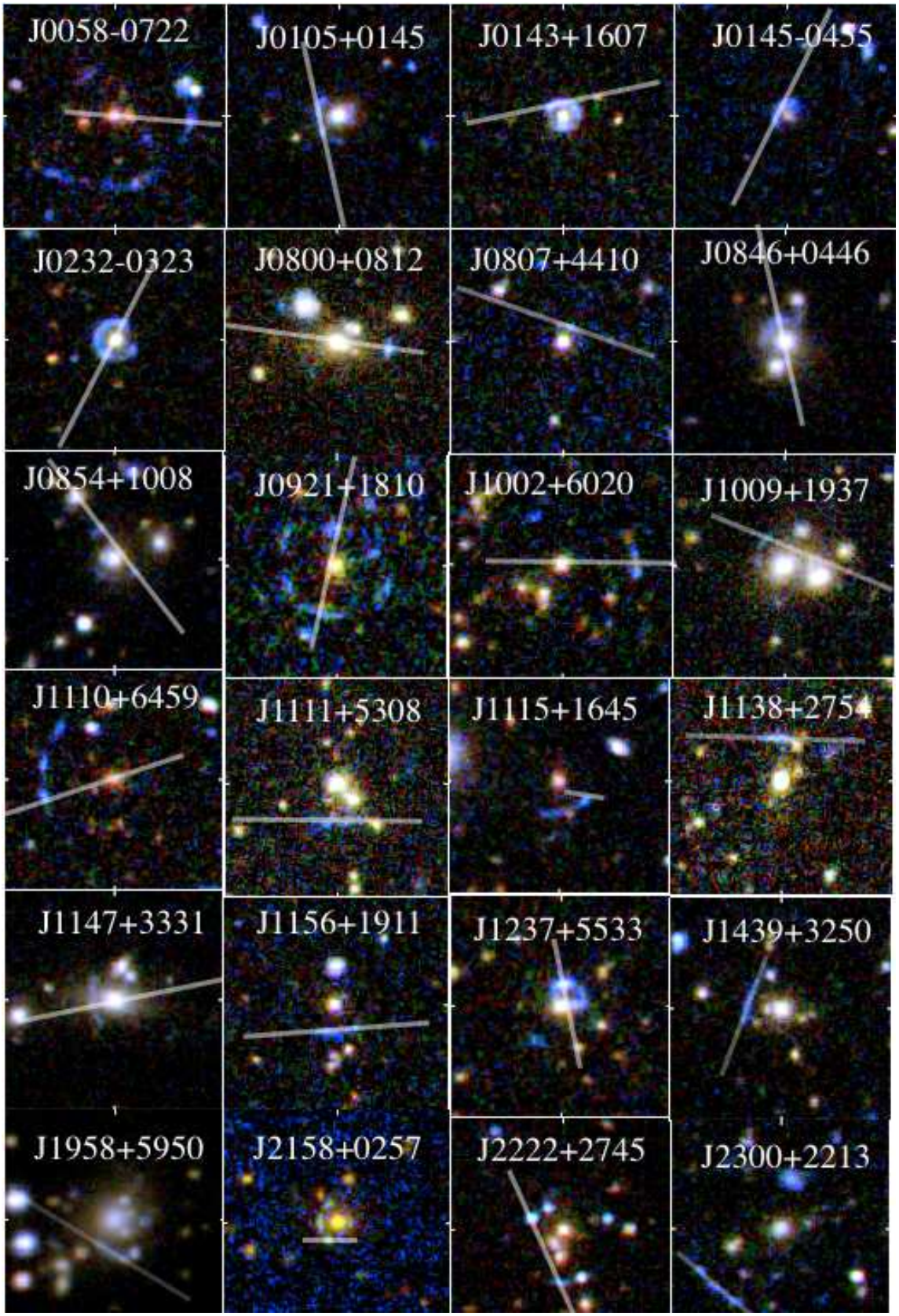

Figure 1. Mosaic of arc+lens systems confirmed in this paper. Each lensed galaxy (except for the arc behind SDSS J1439+3250) has a spectroscopic redshift determined from MMT, Magellan, or Keck. The SDSS IDs are listed at the top of each postage stamp. The images are created from gri-band imaging from SDSS and are 40 arcsec on each side. The slit position used for redshift confirmation is overlaid. For clarity, we do not overlay all slit positions observed in cases where multiple position angles or slit centres were taken.

Lens Name	CSWA-ID	Observatory	Instrument	Configuration	Dates	t_{exp} (ksec)	PA (deg)
SDSS J0058−0722	102	MMT	BCS	300 line/mm	2011 Sep 29	3.6	340
...	...	MMT	RCS	270 line/mm	2013 Jan 21	1.8	85
...	...	MMT	RCS	300 line/mm	2013 Jan 22	4.8	-41
SDSS J0105+0145	165	MMT	BCS	300 line/mm	2011 Sep 30	2.7	2.5
...	...	MMT	BCS	300 line/mm	2012 Dec 12	3.6	5.0
SDSS J0143+1607	116	MMT	BCS	300 line/mm	2011 Sep 29	2.7	105
...	...	MMT	RCS	270 line/mm	2012 Nov 23	1.2	5
SDSS J0145−0455	103	MMT	BCS	300 line/mm	2011 Sep 29	3.6	340
SDSS J0232−0323	164	MMT	BCS	300 line/mm	2011 Sep 29	3.6	330
...	...	Magellan	FIRE	echelle	2012 Feb 15	2.7	58
SDSS J0800+0812	11	MMT	BCS	300 line/mm	2012 Mar 24	1.8	60
...	...	MMT	RCS	270 line/mm	2012 May 01	2.7	60
SDSS J0807+4410	139	MMT	BCS	300 line/mm	2012 Mar 23	3.6	80
SDSS J0846+0446	141	MMT	BCS	300 line/mm	2011 Nov 02	0.6	10
...	...	Keck	DEIMOS	1200 line/mm	2011 Oct 26	2.7	10
...	...	Magellan	FIRE	echelle	2012 Feb 15	1.2	280
SDSS J0854+1008	142	Keck	DEIMOS	1200 line/mm	2011 Oct 26	1.2	30
...	...	MMT	BCS	300 line/mm	2011 Nov 02	2.7	30
SDSS J0921+1810	31	Keck	DEIMOS	1200 line/mm	2011 Oct 26	2.7	120
...	...	MMT	RCS	270 line/mm	2012 Oct 21	2.7	120
SDSS J1002+6020	117	MMT	BCS	300 line/mm	2011 Nov 02	2.7	90
...	...	Keck	DEIMOS	1200 line/mm	2011 Oct 26	1.2	90
...	...	MMT	RCS	270 line/mm	2013 Jan 22	2.7	-94
SDSS J1009+1937	15	MMT	BCS	300 line/mm	2012 Mar 24	2.7	55
SDSS J1110+6459	104	MMT	BCS	300 line/mm	2011 Nov 02	2.7	104
...	...	MMT	BCS	300 line/mm	2012 Mar 24	2.4	104
SDSS J1111+5308	16	MMT	BCS	300 line/mm	2012 Mar 24	2.7	267
SDSS J1115+1645	105	Magellan	FIRE	echelle	2012 Feb 15	2.7	85.2
...	...	MMT	RCS	270 line/mm	2012 Nov 22	0.6	-130
SDSS J1138+2754	17	MMT	BCS	300 line/mm	2012 Mar 24	2.4	85.2
...	...	MMT	RCS	270 line/mm	2012 May 01	2.7	85.2
SDSS J1147+3331	107	MMT	BCS	300 line/mm	2012 Mar 23	3.6	280
...	...	MMT	RCS	270 line/mm	2012 May 01	2.7	280
SDSS J1156+1911	108	MMT	BCS	300 line/mm	2012 Mar 23	3.6	280
...	...	MMT	RCS	270 line/mm	2013 Jan 21	3.6	-20
SDSS J1237+5533	13	MMT	BCS	300 line/mm	2012 Mar 24	1.8	320
...	...	MMT	RCS	300 line/mm	2012 July 06	1.8	320
...	...	MMT	RCS	300 line/mm	2013 Jan 21	3.6	280
SDSS J1439+3250	109	MMT	BCS	300 line/mm	2012 Mar 23	2.7	100
...	...	MMT	RCS	270 line/mm	2013 Jan 22	3.6	-10
...	...	MMT	RCS	300 line/mm	2013 Jan 22	2.4	-10
SDSS J1958+5950	128	MMT	BCS	300 line/mm	2011 Sep 30	2.7	56
...	...	MMT	RCS	1200 line/mm	2012 Jul 06	18	56
...	...	LBT	LUCI	200_H+K (HK)	2012 Nov 06	3.6	-130
...	...	LBT	LUCI	200_H+K (zJ)	2012 Nov 06	2.4	-130
SDSS J2158+0257	163	MMT	BCS	300 line/mm	2011 Sep 30	1.8	20
...		Magellan	FIRE	echelle	2012 Oct 26	2.4	90
SDSS J2222+2745	159	MMT	BCS	300 line/mm	2011 Sep 29	2.7	25
...	...	MMT	RCS	300 line/mm	2012 Aug 23	2.7	25.8,103
...	...	MMT	BCS	300 line/mm	2012 Oct 19	2.7	25
SDSS J2300+2213	111	MMT	BCS	300 line/mm	2011 Sep 29	1.8	45
...	...	MMT	RCS	270 line/mm	2012 Nov 22	3.6	45
...	...	MMT	BCS	300 line/mm	2012 Dec 12	1.8	67
...	...	MMT	RCS	270 line/mm	2013 Jan 21	1.8	50

Table 1. Summary of new spectroscopic observations of SDSS/CASSOWARY lensed galaxies. We have obtained redshifts for all but one of these sources. We list contaminants that we identified in Table 4. The instrument BCS corresponds to the Blue Channel Spectrograph, and RCS refers to the Red Channel Spectrograph. More details are provided in §2.

these redshifts have not appeared in the literature previously. Details of the new sample are provided in Tables 1 and 2. Below we first provide a general overview of the redshift confirmation process (§3.1) before briefly discussing the spectroscopic properties of each system in §3.2.

3.1 Redshift Confirmation

Redshifts were derived through visual examination of the 2D and 1D spectra of each source. We searched the spectra for both emission lines (Lyα or [OII]) and absorption lines. Following the rela-

Lens Name	CSWA-ID	z_{source}	z_{lens}	RA_S	DEC_S	RA_L	DEC_L	Notes
SDSS J0058−0722	102	1.873	0.639†	00:58:47.96	−07:21:58.1	00:58:48.94	−07:21:56.7	Abs
SDSS J0105+0145	165	2.127	0.361†	01:05:19.89	+01:44:59.1	01:05:19.66	+01:44:56.4	Lyα, Abs
SDSS J0143+1607	116	1.499	0.415†	01:43:50.25	+16:07:41.0	01:43:50.12	+16:07:39.0	Abs, Opt
SDSS J0145−0455	103	1.958	0.633†	01:45:04.18	−04:55:42.7	01:45:04.29	−04:55:51.6	Lyα, Abs
SDSS J0232−0323	164	2.518	0.450†	02:32:49.97	−03:23:29.3	02:32:49.86	−03:23:26.0	Lyα, Abs, Opt
SDSS J0800+0812	11	1.408	0.314	08:00:12.37	+08:12:07.0	08:00:13.06	+08:12:08.4	[OII], Abs
SDSS J0807+4410	139	2.536	0.449	08:07:31.37	+44:10:51.3	08:07:31.5	+44:10:48.5	Abs
SDSS J0846+0446	141	1.405	0.241	08:46:47.53	+04:46:09.3	08:46:47.5	+04:46:05.1	Opt
SDSS J0854+1008	142a	1.437	0.298	08:54:28.63	+10:08:11.3	08:54:28.72	+10:08:14.7	[OII]
SDSS J0854+1008	142b	1.271	0.298	08:54:28.97	+10:08:19.9	08:54:28.72	+10:08:14.7	[OII]
SDSS J0921+1810	31	1.487	0.683	09:21:26.46	+18:10:13.7	09:21:25.74	+18:10:17.3	[OII]
SDSS J1002+6020	117	1.114	0.571†	10:02:00.49	+60:20:26.5	10:02:02.51	+60:20:26.3	[OII]
SDSS J1009+1937	15	2.162	0.306	10:09:00.06	+19:37:23.4	10:08:59.77	+19:37:17.5	Lyα
SDSS J1110+6459	104	2.481	0.659†	11:10:19.97	+64:59:44.7	11:10:17.69	+64:59:48.2	Lyα, Abs
SDSS J1111+5308	16	1.945	0.412†	11:11:03.93	+53:08:47.1	11:11:03.30	+53:08:51.8	Abs
SDSS J1115+1645	105	1.718	0.537†	11:15:04.02	+16:45:34.5	11:15:04.39	+16:45:38.6	Opt, Abs
SDSS J1138+2754	17	0.909	0.447†	11:38:09.00	+27:54:39.0	11:38:08.95	+27:54:30.7	[OII], Abs
SDSS J1147+3331	107	1.205	0.212	11:47:23.68	+33:31:53.6	11:47:23.30	+33:31:53.6	[OII]
SDSS J1156+1911	108	1.535	0.543†	11:56:05.5	+19:11:07.3	11:56:05.5	+19:11:12.7	Abs
SDSS J1237+5533	13	1.864	0.410	12:37:36.13	+55:33:47.6	12:37:36.20	+55:33:42.9	Abs
SDSS J1958+5950	128	2.225	0.214†	19:58:35.65	+59:50:53.6	19:58:35.32	+59:50:58.9	Abs, Opt
SDSS J2158+0257	163	2.081	0.291	21:58:43.80	+02:57:26.8	21:58:43.67	+02:57:30.2	Abs, Opt
SDSS J2222+2745	159a	2.309	0.485	22:22:08.58	+27:45:24.7	22:22:08.57	+27:45:35.6	Lyα, Abs
SDSS J2222+2745	159b	2.807	0.485	22:22:09.04	+27:45:37.6	22:22:08.57	+27:45:35.6	QSO
SDSS J2300+2213	111	1.93	0.443†	23:00:18.27	+22:13:18.0	23:00:17.25	+22:13:29.7	Abs

Table 2. Lensed galaxy redshifts in the CASSOWARY catalog obtained through our spectroscopic campaign. Coordinates of the lensed source (RA_s and DEC_s) correspond to rough location where the slit intersects the arc. The lens coordinates (RA_L and DEC_L) reflect the central lensing galaxy. In the far right column, we list the methods of redshift confirmation, where "Abs" implies rest-UV absorption lines, "Opt" implies rest-optical emission lines. Those lensed redshifts with a '†' superscript are not in the SDSS database and are confirmed uniquely via the spectra presented in this paper. The lens redshift for SDSSJ2158+0257 ($z = 0.291$) is provided from VLT observations that will be discussed in Deason et al. (2013, in preparation).

tions presented in Steidel et al. (2010), small offsets were applied to the measured redshifts to account for average kinematic offsets of the interstellar absorption lines and Lyα. If possible, the values presented in Table 2 include these corrections. In this paper, we focus primarily on those systems for which we were able to determine a reliable redshift. At the end of this section, we also briefly discuss interloping objects which satisfied our search algorithm.

The majority of the new lensed sources have been confirmed with the MMT Blue Channel Spectrograph. When bright stellar continua is strongly detected in our spectra, redshift confirmation is easily achieved through identification of prominent far-UV absorption lines and Lyα emission or absorption (Figure 2). The presence of strong Lyα emission enables redshift confirmation in galaxies with weaker continua. As the sensitivity of the MMT blue channel spectra degrades at wavelengths shorter than 3800 Å, each of the five sources confirmed primarily via detection of Lyα emission have redshifts of $z > 2.1$. In cases where Lyα emission is the primary method of redshift identification, we additionally identify weak interstellar absorption lines, thereby confirming the interpretation of the emission line as Lyα.

Reliable redshift identification at $z \lesssim 1.7$ is more difficult with MMT Blue Channel spectroscopy as many of the strongest absorption lines are no longer visible in the spectral window. In this redshift range, most redshifts have been confirmed through detection of [OII] emission with either the MMT Red Channel Spectrograph or Keck/DEIMOS. Of the sample in Table 2, 7 sources were initially confirmed via [OII] emission with redshifts spanning $0.91 < z < 1.49$. For those sources observed with MMT, we typically also identified absorption from Mg II, Fe II, or Al II transitions. For systems observed with DEIMOS, our chosen grating was able to resolve the [OII] doublet, enabling definitive redshift confirmation. For several galaxies, redshifts were first obtained via infrared spectroscopy. In these cases, optical spectra were taken prior to infrared observation, yet in spite of the detection of multiple absorption lines, we were unable to derive a confident redshift. Infrared spectroscopy yielded detection of multiple rest-optical emission lines which enabled confident redshift identification.

Lens redshifts are of course required to derive the intrinsic properties of the lensed source. While many of the lens candidates have redshifts from SDSS spectroscopy, there are a number of early-type systems in our database without spectra. As part of our program with MMT, we obtained spectra of 13 early-type lensing galaxies lacking redshifts. We detected strong continuum and absorption features in each system, allowing us to accurately derive the lens redshifts. These lenses are marked in Table 2.

Throughout our spectroscopic campaign, we also identified a small number of contaminants in our galaxy-galaxy lens selection. Most of the contaminant systems instead correspond to blue galaxies at the same redshift as the red galaxy we had identified as a candidate lens. The coordinates of those systems we confirmed as contaminants are listed in Table 3.

3.2 Notes on Individual Galaxies

Below we provide brief descriptions of the spectra of the galaxies confirmed as part of this survey. When possible, we state redshifts of absorption lines, Lyα emission, as well as the systemic redshifts derived from emission lines in near-IR spectroscopy.

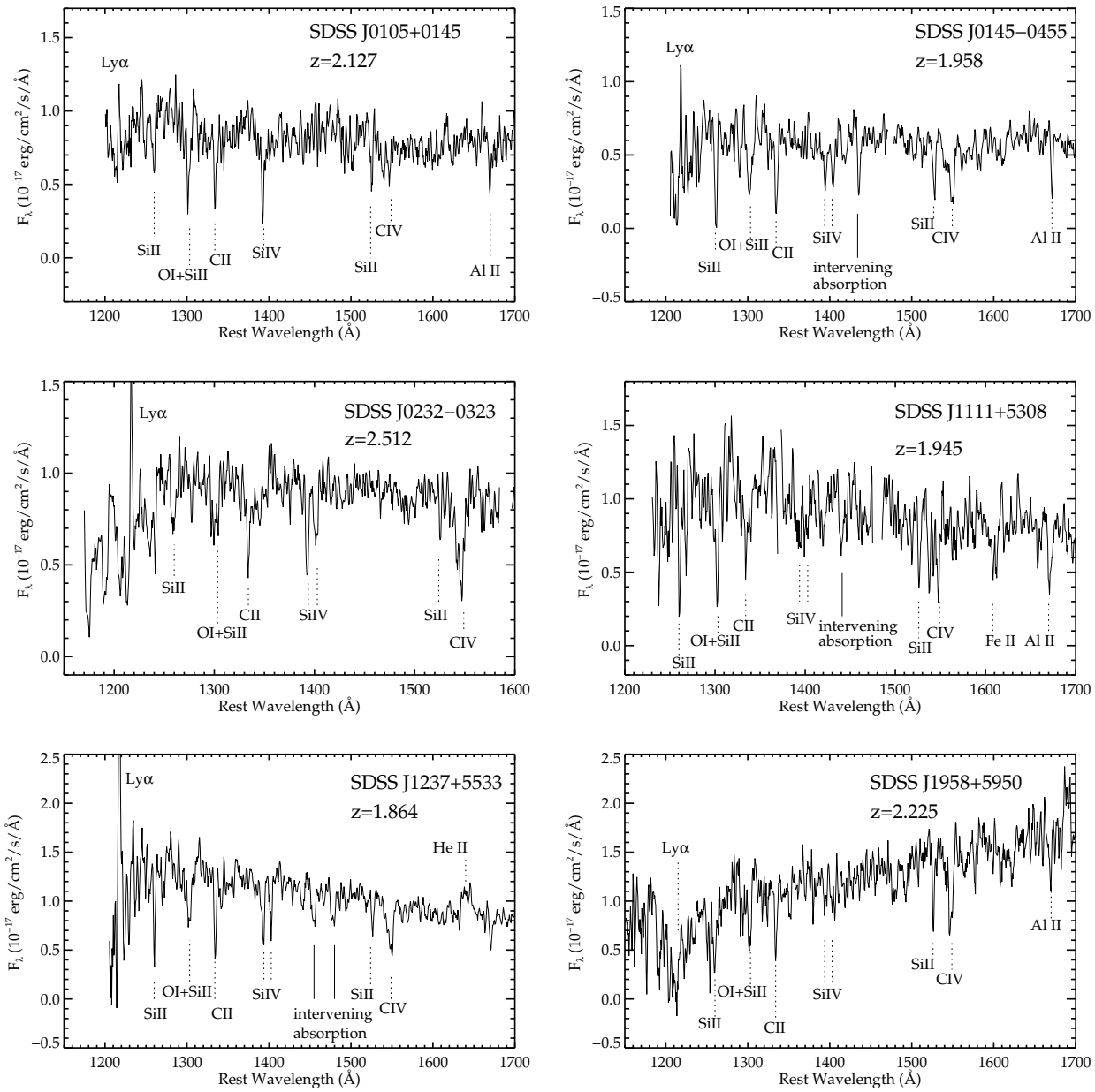

Figure 2. Examples of MMT spectra of newly-confirmed gravitationally lensed galaxies located within SDSS as part of the CASSOWARY survey. Owing to the very bright optical magnitudes ($r \simeq 19-22$), exposure times of just 30-45 min with the Blue Channel Spectrograph (see Table 1) are sufficient to reveal many absorption lines (denoted with dotted lines) throughout the rest-frame UV. We also point out several likely intervening absorption systems identified in the 2D and 1D spectra.

SDSS J0058−0722, z=1.87: This system is composed of a number of blue arcs around three bright early type galaxies at wide separation ($\simeq 15''$). We detected the brightest source continuum flux from the arc to the west of the lenses. Redshift confirmation is achieved through identification of absorption lines (Si IV, Si II, CIV, Fe II, Al II) in the MMT blue channel spectrum. We determined the redshift of the absorbing gas (z=1.872) from Al II, the most isolated absorption line in the blue channel spectrum. The red channel spectrum shows absorption at the observed wavelengths expected for Fe II λ2344 and Fe II $\lambda\lambda$2374,2382. As the lens redshift is not in the SDSS database, we have obtained additional exposures with the MMT slit oriented along the three central group members. We measure a lens redshift of $z = 0.639$ through identification of absorption lines in the MMT spectrum.

SDSS J0105+0145, z=2.13. Strong stellar continuum and prominent absorption lines are seen in the MMT blue channel spectrum of the arc behind SDSS J0105+0145 (Figure 2). We measure a redshift of $z = 2.126$ from CII λ1334 absorption. Weak Lyα emission is tentatively detected with $z_{\mathrm{Ly}\alpha} = 2.131$. The mean kinematic offset between the blueshifted absorbing gas and Lyα emission is 540 km s^{-1}. Higher S/N data will be required to confirm the properties of Lyα emission. We note that the apparent strength of SIV absorption is artificially amplified by a negative skyline resid-

ual. We measure the lens redshift ($z = 0.361$) with a separate MMT exposure.

SDSS J0143+1607, z=1.50. Strong continuum is detected in the MMT blue channel spectrum, but some blending with the lens ($\simeq 2$ arcseconds away from the centre of the slit) is present. Nevertheless we detect CIVλ1549 in absorption as well as weak absorption corresponding to Al II λ1671. The CIV absorption line redshift in the MMT spectrum is $z = 1.500$. We detect [OII] emission from two components of the source in our MMT red channel spectrum. The line is unresolved at the resolution of our spectrum. Assuming a flux-weighted mean [OII] wavelength of 3728.3 Å, we derive a redshift of $z = 1.500$ from the line detection. As the central lens galaxy redshift was not in the SDSS database, we obtained its redshift ($z = 0.415$) with an MMT red channel spectrum.

SDSS J0145-0455, z=1.96: We detect strong continuum and absorption in the spectrum of SDSS J0145-0455 (Figure 2). We measure a mean low ionisation absorption line redshift of $z = 1.957$. Weak Lyα emission is detected, but the rest-frame EW (~ 6 Å) is fairly uncertain owing to the difficulty in characterising the continuum at wavelengths shorter than 3800 Å. CIII]λ1909 emission is detected with a measured rest-frame EW of 1.5 Å, comparable to that seen in the composite $z \simeq 3$ LBG spectrum of Shapley et al. (2003).

We detect pronounced absorption from an intervening system at observed wavelength 4244 Å (corresponding to rest-wavelength 1435 Å in the frame of the lensed $z = 1.96$ galaxy). We cannot confidently determine the redshift of the absorption system with our current low resolution spectra. If due to Mg II absorption, it would imply a redshift of $z = 0.52$ and might indicate some spectral blending between Fe II λ2600 absorption (from the intervening system) and CIIλ1334 absorption from the $z = 1.96$ source. Likewise, if the absorption at 4244 Å is due to CIV at $z = 1.74$, then it might signal spectral blending between Al II λ1671 (from the intervening system) and CIVλ1549 in the $z = 1.96$ reference frame. We do note the presence of weak absorption at 4188 Å, as might be expected from Si IIλ1526 at $z = 1.74$. The finally possibility we consider is that the absorption at 4244 Å corresponds to Fe IIλ2600 at $z = 0.63$. This possibility is particularly intriguing, as this redshift is identical to the redshift of the galaxy responsible for lensing, potentially signalling some residual low ionisation gas associated with the early-type system. In this case, we would expect spectral blending from Mg II absorption (at $z = 0.63$) at the wavelength of CIV in the $z = 1.96$ reference frame. Higher resolution spectra will help clarify the situation.

SDSS J0232−0323, z=2.51 As seen in Figure 1, the MMT slit targeting SDSS J0232−0323 covers the source in two locations, to the NW and SE of the lens. We detect Lyα emission and interstellar absorption lines from the source on both sides (Figure 2). The escaping Lyα radiation has a mean redshift of $z_{\rm Ly\alpha}$=2.515. From the unblended CIIλ1334 absorption line, we find that the low ionisation absorbing gas has a mean redshift of $z = 2.510$. We establish a systemic nebular redshift of $z = 2.512$ from detection of [OIII]λ5007 in our Magellan/FIRE spectrum. These data imply that the low ionisation gas has a mean outflow velocity of -160 km s^{-1} and that the Lyα radiation escapes with a mean velocity of 250 km s^{-1} with respect to systemic.

SDSS J0800+0812, z=1.41: Both blue and red channel data were obtained for SDSS J0800+0812, providing spectral coverage between 3600 and 9070 Å. Absorption from Fe IIλ2600 and Mg II$\lambda\lambda$2796,2803 is seen in the MMT red channel spectra, indicating a redshift of $z = 1.407$ for the absorbing gas. Additionally, we detect strong [OII] emission (rest-frame EW of 60 Å) at 8983 Å, revealing a nebular redshift of $z = 1.408$ assuming that the rest-frame centroid of the unresolved [OII] doublet is 3728.3 Å.

SDSS J0807+4410, z=2.54: We detect weak stellar continuum, Lyα absorption, and multiple interstellar absorption lines in our MMT blue channel spectrum of the faint arc around SDSSJ0807+4410. The low ionisation absorbing gas has a mean redshift of $z = 2.540$ in the MMT spectra. Its close proximity to the lens ($\simeq 3$ arcsec to the centre of the elliptical galaxy) results in some blending at wavelengths greater than 5500 Å.

SDSS J0846+0446, z=1.43: Redshift confirmation was first achieved through the detection of numerous emission lines with DEIMOS. In addition to [OII] and [Ne III]λ3869, we identified Hydrogen Balmer series lines Hϵ, H8, H9, H10, H11, H12. Subsequent infrared observations with Magellan/FIRE yielded many further rest-optical emission features, including the temperature-sensitive [OIII]λ4363 auroral line (Figure 3) and the electron density sensitive [SII] emission lines. We derived a nebular redshift of $z = 1.425$ from the observed hydrogen Balmer emission lines in the FIRE spectrum. The observed spectrum points to emission from a very young and metal-poor system. The detection of so many emission lines will enable a comprehensive analysis of the physical conditions of the ionised gas. We will briefly discuss this source in more detail in §5.1. A complete discussion will be presented in a future paper (Stark et al. 2013, in preparation).

SDSS J0854+1008, z=1.44 and z=1.27. DEIMOS observations of the SDSS J0854+1008 system yielded detections of [OII] emission at two different redshifts. We detect resolved [OII] emission from the blue arc to the NE of the lens (see Figure 1), yielding a nebular redshift of $z = 1.271$. We also detect faint emission at 3868 Å that we tentatively identify as [Ne III]λ3869. In addition to this source, the DEIMOS slit also passes through a fainter ring of blue emission surrounding the lens. The slit intersects the ring to the NE and SW of the lens. We detect resolved [OII] emission at 9080, 9086 Å in both images, confirming the redshift of this second source as $z = 1.436$.

SDSS J0921+1810 z=1.49: Redshift confirmation is achieved through detection of [OII] emission in both the DEIMOS and MMT red channel spectra. The doublet is fully resolved in the 1200 line/mm grating DEIMOS spectrum. We derive a nebular redshift of $z = 1.486$ from the centroids of the [OII] doublet. We do detect stellar continuum in the DEIMOS spectrum, but the narrow wavelength range does not cover strong absorption features. The shallower MMT spectrum does not reveal continuum, so at this stage, we have no information on the properties of the circumgalactic gas around SDSS J0921+1810.

SDSS J1002+6020, z=1.11: We detect [OII] emission in each of the three spectra taken of the arc lensed by the galaxy SDSS J1002+6020. Based on the wavelength of [OII] emission, we confirm a redshift of $z = 1.114$ for the source. We detect emission at the wavelength of Hδ and Ne III λ3869 in the MMT red channel spectrum. The MMT blue channel spectrum shows absorption at the observed wavelengths corresponding to Fe II λ2344 and Fe II $\lambda\lambda$2374, 2382.

SDSS J1009+1937, z=2.16: Lyα emission is present at 3850 Å in the MMT blue channel spectrum, indicating a Lyα redshift of 2.167. While the continuum S/N is not as strong as in other sources, we confirm the presence of the Si IIλ1526, and CIVλ1549 absorption lines. The CIV centroid is consistent with a redshift $z = 2.158$. Higher S/N absorption line spectra are required to accurately quantify the kinematics of the absorbing gas.

SDSS J1110+6459, z=2.48: Lyα emission is clearly visible in the MMT spectrum of SDSS J1110+6459. The equivalent width is

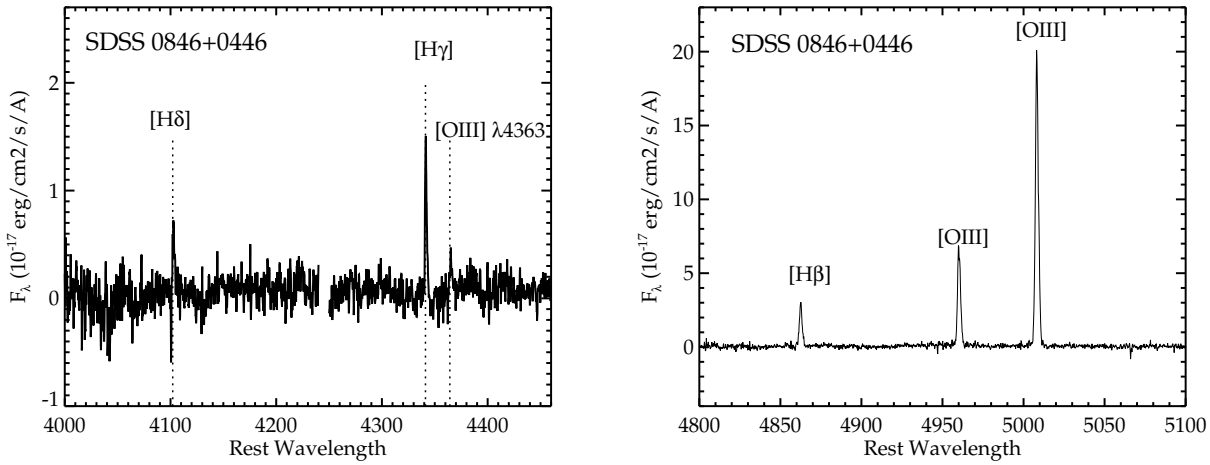

Figure 3. Portion of Magellan/FIRE near-IR spectra of SDSS J0846+0446, a lensed strong emission line $z = 1.43$ galaxy in our new sample. Detection of the [OIII]λ4363 emission line (left panel) enables measurement of the electron temperature and reflects the low metallicity (0.2 $Z_\odot$) of the nebular gas. The rest-frame EW of [OIII]λ5007 ($\gtrsim$ 320 Å; right panel) is similar to those of extreme line emitting galaxies found in grism and imaging surveys, while the EW of Hydrogen Balmer lines points to a young stellar population. With numerous emission lines detected across the optical and near-IR, future analysis of this source will yield new insight into the nature of the extreme line emitting population.

moderate in strength (rest-frame $EW \simeq 3$ Å) with a redshift of $z = 2.483$. We detect absorption from OI+SiIIλ1303, CIIλ1334, and Al II λ1671 with a mean redshift of $z = 2.476$.

SDSS J1111+5308, z=1.95: Strong continuum and absorption are detected in the MMT blue channel spectrum, as is seen in Figure 2. The mean redshift for the low ionisation absorbing gas is $z = 1.946$. We detect absorption at 4245 Å which would correspond to 1441 Å if in the rest-frame of the lensed source toward SDSS J1111+5308. As no absorption is expected at this rest-wavelength, this feature is likely produced by gas associated with a foreground system. Higher resolution data will be required to determine the redshift of the intervening system.

SDSS J1115+1645, z=1.72: Our initial MMT optical spectra of this target suffered contamination from a foreground red galaxy (see postage stamp Figure 1), making redshift confirmation difficult. After placing the FIRE slit directly on the bright blue knot to the SW of the lens, we were able to confirm the systemic redshift as $z = 1.717$ through detection of Hα, Hβ, and [OII] emission. Emission from [OIII]λ5007 and 4959 falls in the low transmission region between the J and H-bands and is not detected. No redshift existed for the lens in the SDSS database. After redshift confirmation with FIRE, we therefore revisited the system with MMT to acquire the lens redshift. By orienting an MMT red channel slit to include both source and lens, we were able to identify lens absorption features indicating a redshift of $z = 0.537$. We also identified continuum from the $z = 1.72$ source, but the S/N was not sufficient to reliably characterize Mg II and Fe II absorption lines. We note that observations of SDSS J1115+1645 in Bayliss (2012) reveal an additional lensed source at $z = 3.463$.

SDSS J1138+2754 z=0.91: Extended [OII] emission is detected in both blue and red channel spectra, revealing the source redshift as $z = 0.909$, as previously reported in Wutys et al. (2012). We measure a rest-frame [OII] EW of 60 Å, similar to SDSS J0800+0812. We also detect extended [Ne III] in the red channel spectrum. We do not detect strong absorption from Fe II or Mg II transitions.

SDSS J1147+3331, z=1.21: Redshift confirmation ($z = 1.205$) was obtained through detection of [OII] emission with our MMT red channel spectrum. The brightness of the lens ($z = 16.1$) and its reasonably close proximity to the source (see Figure 1) cause significant blending in the MMT spectrum. While we detect faint stellar continuum (particularly in the blue channel data), it is difficult to reliably characterise absorption lines as a result of the blending.

SDSS J1156+1911, z=1.54: Strong continuum in the MMT blue channel spectrum. We detect absorption features at $\sim$ 3870, 3927, 4076, and 4236 Å. The most likely classification of these features is Si II λ1526, CIV λ1549, Fe II λ1608, and Al I Iλ1671, respectively. The centroids of these absorption features imply a redshift of $z = 1.535$ for the absorbing gas. In the same spectrum, we note the presence of weak low S/N emission at 4226 and 4839 Å (OIII] λ1667 Åand CIII] λ1909 Å) and weak absorption at 5940 Åpossibly corresponding to Fe II λ2344. The S/N of the red channel is lower than that of our blue channel spectrum, but we do tentatively note absorption at 7090-7080 Å, as expected from the Mg II doublet.

SDSS J1237+5533, z=1.87: In addition to being among the brightest lensed galaxies in our sample, the arc toward SDSS J1237+5533 is fairly compact, translating into a very high surface brightness and easily detectable continuum emission. Strong absorption lines are readily apparent across the rest-UV (Figure 2). We obtain a redshift of $z = 1.863$ from CII λ1334 and $z = 1.868$ from Lyα λ1216. The EW of Lyα emission is uncertain due to the weak continuum signal at 3400 Å. The velocity offset between Lyα emission and CII absorption is 570 km s^{-1}, consistent with expectations from spectra at $z \simeq 2-4$ (Shapley et al. 2003; Steidel et al. 2010; Jones et al. 2012). In addition to Lyα, we tentatively identify emission from He IIλ1640 and CIII]λ1909. The rest-frame equivalent width of CIII]λ1909 (4 Å) is greater than the equivalent width measured in the $z \simeq 3$ composite spectrum but consistent with that seen in the subset of galaxies with strong Lyα emission (Shapley et al. 2003). We identify intervening absorption at λ =4167 and 4229 Å. Possible interpretations for these features include Si IIλ1526 and CIVλ1549 absorption at $z = 1.73$ or Fe IIλ2344 and

Contaminant Name	RA	DEC	z_{cont}
SDSS J0840+1052	08:40:21.0	+10:52:12.7	0.048
SDSS J0013+3512	00:13:31.9	+35:12:21.0	0.144, 0.269
SDSS J1046+1048	10:46:01.1	+10:48:52.7	0.247
SDSS J0206+0448	02:06:38.9	+04:48:03.8	0.262
SDSS J1502+2920	15:02:36.6	+29:20:53.9	0.245
SDSS J1421+4143	14:21:55.3	+41:43:20.9	0.228

Table 3. Contaminants in CASSOWARY sample. The redshift of the blue galaxy we had identified as a candidate arc is listed as z_{cont}. Coordinates give the location of the red central galaxy.

Fe II$\lambda\lambda$2374,2382 absorption at $z = 0.78$. Higher resolution and higher S/N spectroscopy will be required to confirm the redshifts of the intervening absorption systems and disentangle their contribution to the absorption associated with the CGM of the $z = 1.87$ lensed galaxy.

SDSS J1439+3250: We detect continuum and several pronounced absorption lines in the MMT blue channel spectrum of the triplet arc system to the southwest of the SDSS J1439+3250 lens. The redshift identification appears complicated by the presence of intervening absorption systems. We currently identify a number of possible redshift solutions, including $z = 2.15$ based on absorption at 3970, 4202, 4806, and 4879 Å which would correspond to Si II λ1260, CII λ1334, SiII λ1526, and CIV λ1549. The red channel spectra (Table 1) do not show strong absorption features, perhaps due to limited exposure time and reduced transparency during the observations. We note that the absorption seen at 3970 Å in the blue channel spectra might instead reflect absorption from the Mg II doublet at the redshift of the lens ($z = 0.418$). If confirmed, this would indicate the presence of neutral gas associated with the central lens or satellite galaxies. Higher S/N spectra are required to finalise the redshift of the source and the interpretation of the absorption lines.

SDSS J1958+5950, z=2.22: At r=19.6, this is one of the brightest lensed galaxies known in SDSS. Multiple strong absorption lines are detected in the MMT spectrum (Figure 2). We derive a redshift of $z = 2.222$ from CII λ1334 absorption, consistent with the redshifts derived from the other low ionisation absorption lines. While the lens is 6 arcsec away from the slit centre, the red continuum spectral slope possibly points to some low level contamination from one of the lensing galaxies. However the presence of strong absorption lines from the $z = 2.22$ galaxy suggests that contaminating stellar continuum is not dominant in the wavelength regime we are considering. Higher resolution imaging will be required to decipher the UV continuum slope of the components of the arc. As detailed in Table 1, we have also obtained near-IR spectra covering 0.9 to 2.4μm with LBT. Multiple emission lines and continuum are detected in the spectrum. We derive a mean systemic redshift of $z = 2.225$ from Hα and [OIII]λ5007 emission. The low ionisation absorption lines detected with MMT are therefore blueshifted by 200-300 km s^{-1} from the systemic redshift.

SDSS J2158+0257, z=2.08 Multiple absorption lines are detected throughout the MMT blue channel spectrum. We derive a mean low ionisation absorption line redshift of $z = 2.079$ from CII λ1334 and OI+SiII λ1303. Lyα is seen in absorption. Strong emission lines are present throughout the rest-frame optical with Magellan/FIRE. The systemic redshift determined from Hβ and Hα is $z = 2.081$, indicating that the average velocity of the low ionisation absorbing gas is -200 km s^{-1}. The lens redshift ($z = 0.290$) is confirmed through VLT/FORS spectroscopy (Deason et al. 2013, in preparation).

SDSS J2222+2745, z=2.30 and z=2.81: We confirmed a lensed galaxy at $z = 2.31$ and a quasar at $z = 2.81$ in the first spectrum of we took of the SDSS J2222+2745 system. Both sources were recently reported in Dahle et al. (2012). The galaxy redshift is easily identified via the presence of Lyα emission and weak interstellar absorption lines. The Lyα rest-frame EW is 20 Å, the strongest in our sample. The low ionisation absorbing gas ($z = 2.298$) is blueshifted with respect to the escaping Lyα radiation ($z_{Ly\alpha} = 2.300$), consistent with a kinematic offset of 250 km s^{-1}.

The QSO toward SDSS J2222+2745 is easily confirmed in our MMT spectra through broad Lyα and CIV emission. Lyα emission is extended over 16 arcseconds. As detailed in Dahle et al. (2012), the lensed quasar is multiply-imaged with 6 separate images reported. Over the last year, we have obtained spectra for 4 quasar images with MMT. The strong continuum in the quasar allow us to characterise the spatial extent of the absorbing gas from the nearby $z = 2.30$ lensed galaxy. While this is common in QSO absorption systems, the brightness of the arc ($g \simeq 21$; Dahle et al. 2012) enables unique constraints on the absorbing gas along the line of sight to the galaxy. We will provide a brief discussion of this particular system in §5.

SDSS J2300+2213, z=1.93: We have observed the arcs in SDSS J2300+2213 on numerous occasions with MMT. We identify strong continuum and a number of absorption lines. In the MMT blue channel data, we identify absorption lines at $\simeq$3816, 3906, 4473, 4543, and 4893 Å, which appears to correspond to absorption from OI+SiIIλ1303, CII λ1334, Si II λ1526, and CIV λ1549. and Al II λ1671 absorption at $z = 1.93$. The S/N of the detected absorption lines does not permit a more precise redshift measurement. We also see absorption at $\simeq 4140$ Å which we might stem from an intervening absorption systems. In the same blue channel spectrum, we also see absorption at the observed wavelength corresponding to and Fe II $\lambda\lambda$2374, 2382. At $z = 1.93$, the Fe II λ2344 and Fe II $\lambda\lambda$2586,2600 transitions overlap with the atmospheric B-band and A-band absorption features and so cannot be used to independently verify the redshift. Using our MMT red channel data, we do note the presence of absorption at $\simeq 8200$ Å, which would correspond to Mg II doublet at $z = 1.93$. We have determined the redshift of the central lensing galaxy ($z = 0.443$) using a combination of red channel and blue channel spectra.

4 PHYSICAL PROPERTIES OF CASSOWARY LENSED SOURCES

We present the total CASSOWARY spectroscopic sample (§4.1). Derivation of physical properties of course requires estimates of the source magnification which we describe in §4.2. Using these measurements, we discuss the typical star formation rates and stellar masses of lensed sources in our sample (§4.3).

4.1 Total spectroscopic sample

We have added spectra for 25 bright objects to our redshift database of lensed sources in SDSS. With the exception of the lensed QSO and galaxy system behind SDSS J2222+2745 (recently reported in Dahle et al. 2013) and the $z = 0.91$ arc toward SDSS 1138+2754 (Wuyts et al. 2012), the redshifts are new additions to the literature. Several of the new sources had appeared (without spectroscopic

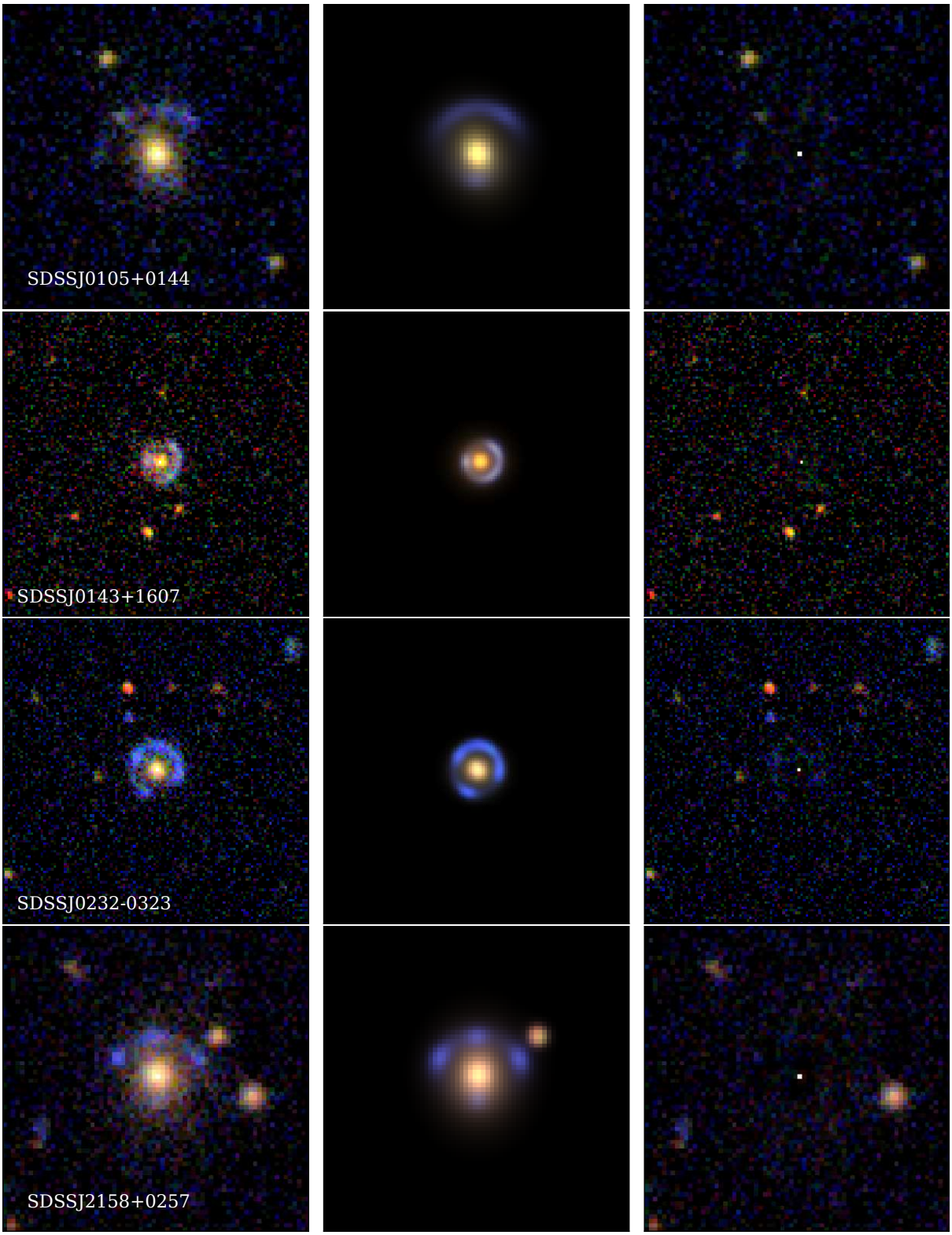

Figure 4. Examples of lens models for newly-confirmed CASSOWARY systems that demonstrate the robustness of our modelling scheme. The left panel shows the SDSS images, the middle panel shows the model of the system, and the right panel shows the residuals when the model is subtracted from the data. Details of the modelling procedure are provided in §4.2 and lens model parameters can be found in Table 4.

confirmation) in Wen et al. (2011), and several are mentioned as part of the Sloan Giant Arcs Survey (SGAS) in Bayliss (2012).

The total CASSOWARY SDSS spectroscopic catalog (now numbering 55 sources) is listed in Table 4. Many objects in this sample are of course not unique to the CASSOWARY selection. The Sloan Bright Arcs Survey (SBAS) has identified (and provided initial confirmation) for a significant number of galaxies listed in Table 4 (see reference column in the table) using an algorithm selecting blue arcs around both luminous red galaxies and brightest cluster galaxies (e.g., Allam et al. 2007; Kubo et al. 2010). As mentioned above, there is also overlap with the SGAS sample. Nine of the CASSOWARY targets listed in Table 4 were observed in Bayliss et al. (2011), and we expect to see more overlap as the entire SGAS sample is released.

4.2 Typical source magnification factors

We use the gri imaging data from SDSS DR8 to fit each of the objects with singular isothermal ellipsoid (SIE; Kormann et al. 1994) lens models. In doing so, we use the method described in Auger et al. (2011) extended to multiple filters and (potentially) multiple foreground light distributions. To summarise, the light from neighbouring foreground galaxies is modelled as Sersic surface brightness distributions, as is the light from the background source. The same light and mass model is fit to each of the filters simultaneously, although the amplitudes of the surface brightness profiles are allowed to vary between the different bands. We also allow for small offsets between the mass and the light of the primary lensing galaxy, and we require the axis ratio of the mass distribution to be greater than 0.2. In all cases we use a single surface brightness component for the background source; when multiple sources are present, we model the source with the largest number of images. We are unable to find well-constrained models in 22 out of 51 lens systems due to the quality of the SDSS imaging; for the remaining 29 systems we find typical source magnifications of 5-10$\times$. We list the relevant model parameters in Table 4 for those systems which we fit. The magnification factors quoted refer to the ratio of total flux to intrinsic flux. We note that our magnification estimates for several well-known systems (SDSS J1148+1930 and SDSS J1206+5142) are consistent (to within a factor of two) with previous results based off of deeper imaging (e.g., Dye et al. 2008; Jones et al. 2012b). In order to fully exploit detailed follow-up spectroscopy, it will be crucial that we obtain higher quality imaging to improve the quality of the modelling in all systems.

4.3 Average global properties

Equipped with the average magnification factors described in section 4.2, we can estimate the SFRs and stellar masses of our sample of lensed galaxies. We will postpone a source-by-source analysis until we have acquired deeper optical and near-IR imaging data. Our primary goal here is merely to establish the average properties likely spanned by the spectroscopic sample.

We can crudely estimate the range of SFRs from the optical photometry from SDSS. Given the range of magnification factors (typically 5-10$\times$ but as large as $\sim 30\times$), we estimate that the range of optical magnitudes of the $z \simeq 2$ subset typically translate into (unlensed) UV absolute magnitudes in the range $M_{UV} \simeq -22$ to -21. This corresponds to roughly 1-3 $L^{\star}_{UV}$ at $z \simeq 2$ (Reddy et al. 2012b). To estimate the corresponding SFR, we need to account for dust extinction. In absence of direct constraints of the rest-frame far IR continuum, this is often done through measurement of the reddened UV continuum slope. Given the source selection, most of the systems in our sample are fairly blue with $(g-r) \simeq 0.0-0.1$ which implies UV spectral slopes in the range $\simeq -2.0$ to -1.7, somewhat bluer than average for this luminosity range (e.g., Bouwens et al. 2009; Reddy et al. 2012a). Adopting the Meurer relation for our $z \simeq 2$ sample (Reddy et al. 2010; 2012a), we infer that *typical* star formation rates in the lensed SDSS $z \simeq 2$ sample likely span the range 20-100 $M_{\odot}$ yr^{-1}. Individual systems within the sample will of course deviate from these values owing to the distribution functions of magnification, UV slope, and SFR to UV luminosity ratios present in the sample.

Knowledge of the stellar masses of the lensed galaxies will have to wait for deeper near-IR coverage. While three of the sources in Table 1 are in the Large Area Survey of the UKIRT Infrared Digital Sky Survey (UKIDSS), they are not detected with enough significance in the K-band to enable stellar mass estimates. For the sake of comparison, we instead estimate the range of stellar masses of our sample through the well-established relationship between $M_{\star}$ and M_{UV} at $z \simeq 2$ (Reddy et al. 2012b). Given our estimates of the magnification distribution and the observed optical magnitudes, the stellar mass of galaxies in the $z \simeq 2$ subset is likely to be in the range $\simeq 10^{10}$-10^{11} $M_{\odot}$, similar to the masses inferred for well-studied examples in Table 4. If the blue (g-r) colours in our sample reflect younger ages, this might point to slightly lower stellar mass to light ratios than typical objects used in the Reddy et al. (2012b) calibration, indicating that the lensed systems might tend to lie at the lower end of the quoted mass range.

Clearly improved multi-wavelength imaging is a crucial requirement for fully exploiting this unique dataset. Not only does such imaging provide the necessary depth to accurately characterise the observed source SED and improve estimates of total magnification factors, but it also delivers the necessary constraints to accurately interpret the resolved spectroscopic maps that we are pursuing with integral field spectrographs. As demonstrated in our earlier work (Jones et al. 2012b), only with sufficient image quality can the source plane be reliably reconstructed.

5 DISCUSSION

The sample presented in this paper will provide a major stimulus to efforts to use lensed galaxies as detailed probes of galaxy formation at high redshift. Detailed optical and near-infrared follow-up of this new population is now underway and will be discussed in future papers. In the following we provide an initial exploitation of the sample using the existing data.

5.1 A lensed extreme emission line galaxy

Most of the optically-bright lensed $z \simeq 2-3$ galaxies that have been studied in detail are broadly similar in their properties to typical systems within the population of UV-continuum selected galaxies (e.g., Shapley 2011 and references therein). But as the sample of bright lensed galaxies increases, we expect to find outliers that offer unique insight into galaxy formation at high redshift.

The $z = 1.43$ arc in SDSS J0846+9446 appears to be such a source. While this is by no means the brightest continuum source in our sample, the EWs of the Balmer lines are much larger than are typically seen in UV-selected galaxies (see Figure 3), allowing us to detect Hα through H12 with the short 20 min integration detailed

SDSS ID	CSWA ID	RA	DEC	z_L	z_S	R_{ein} ($''$)	μ	Reference
SDSS J0022+1431	21	00:22:40.92	+14:31:10.4	0.380	2.730	3.3	9.9	[1]
SDSS J0058−0721	102	00:58:48.95	−07:21:56.7	0.639	1.873	...	...	This paper
SDSS J0105+0144	165	01:05:19.65	+01:44:56.4	0.361	2.127	3.5	5.4	This paper
SDSS J0143+1607	116	01:43:50.13	+16:07:39.0	0.415	1.499	2.7	10.7	This paper
SDSS J0145−0455	103	01:45:04.29	−04:55:51.6	0.633	1.958	1.9	4.7	This paper
SDSS J0146−0929	22	01:46:56.01	−09:29:52.5	0.440	1.944	11.9	9.7	[18]
SDSS J0232−0323	164	02:32:49.87	−03:23:26.0	0.450	2.518	3.7	20.8	This paper
SDSS J0800+0812	11	08:00:13.06	+08:12:08.4	0.314	1.408	...	...	This paper
SDSS J0807+4410	139	08:07:31.51	+44:10:48.5	0.449	2.536	2.1	3.8	This paper
SDSS J0827+2232	23	08:27:28.83	+22:32:53.9	0.349	0.766	...	...	[2]
SDSS J0846+0446	141	08:46:47.46	+04:46:05.1	0.241	1.405	3.4	5.5	This paper
SDSS J0851+3558	30	08:51:26.50	+35:58:13.8	0.272	0.919	...	...	[18]
SDSS J0854+1008	142	08:54:28.73	+10:08:14.7	0.298	1.271, 1.437	4.2	4.0	This paper
SDSS J0900+2234	19	09:00:02.64	+22:34:04.9	0.489	2.033	7.9	6.5	[3]
SDSS J0901+1814	4	09:01:22.37	+18:14:32.3	0.346	2.259	...	...	[4]
SDSS J0921+1810	31	09:21:25.74	+18:10:17.3	0.683	1.487	...	...	This paper
SDSS J0952+3434	40	09:52:40.22	+34:34:46.1	0.349	2.190	4.2	3.2	[5]
SDSS J0957+0509	35	09:57:39.19	+05:09:31.9	0.440	1.823	5.4	3.7	[5]
SDSS J1002+6020	117	10:02:02.52	+60:20:26.3	0.575	1.114	...	...	This paper
SDSS J1008+1937	15	10:08:59.78	+19:37:17.5	0.306	2.162	...	...	This paper
SDSS J1038+4849	2	10:38:43.58	+48:49:17.7	0.426	0.972, 2.20	...	...	[6], [17]
SDSS J1049+3544	33	10:49:23.39	+35:44:41.0	0.300	1.000	3.5	10.5	[18]
SDSS J1110+6459	104	11:10:17.69	+64:59:48.2	0.659	2.481	11.3	8.1	This paper
SDSS J1111+5308	16	11:11:03.68	+53:08:54.9	0.412	1.945	...	...	This paper
SDSS J1113+2356	26	11:13:10.65	+23:56:39.5	0.336	0.770	...	...	[7]
SDSS J1115+1645	105	11:15:04.39	+16:45:38.6	0.537	1.718	4.6	3.4	This paper
SDSS J1133+5008	12	11:33:13.17	+50:08:40.1	0.394	1.544	...	...	[8]
SDSS J1137+4936	7	11:37:40.06	+49:36:35.5	0.448	1.411	2.8	8.5	[7]
SDSS J1138+2754	17	11:38:08.95	+27:54:30.7	0.447	0.909	6.2	4.7	[19]
SDSS J1147+3331	107	11:47:23.30	+33:31:53.6	0.212	1.205	4.6	8.1	This paper
SDSS J1148+1930	1	11:48:33.14	+19:30:03.1	0.444	2.379	5.1	28.7	[9]
SDSS J1156+1911	108	11:56:05.46	+19:11:12.7	0.543	1.535	...	...	This paper
SDSS J1206+5142	6	12:06:02.09	+51:42:29.5	0.433	2.000	3.9	14.9	[10]
SDSS J1207+5254	36	12:07:35.91	+52:54:59.2	0.270	1.926	...	...	[5]
SDSS J1209+2640	8	12:09:23.69	+26:40:46.7	0.558	1.018	8.4	7.0	[11]
SDSS J1226+2152	38	12:26:51.69	+21:52:25.5	0.420	2.923	...	...	[12]
SDSS J1237+5533	13	12:37:36.20	+55:33:42.9	0.410	1.864	...	...	This paper
SDSS J1240+4509	3	12:40:32.29	+45:09:02.8	0.274	0.725	2.9	5.7	[6]
SDSS J1244+0106	5	12:44:41.01	+01:06:43.9	0.388	1.069	...	...	[14]
SDSS J1318+3942	37	13:18:11.51	+39:42:27.0	0.475	2.944	...	...	[5]
SDSS J1343+4155	28	13:43:32.85	+41:55:03.5	0.418	2.093	...	...	[3]
SDSS J1441+1441	20	14:41:49.15	+14:41:20.6	0.741	1.433	3.0	6.3	[15]
SDSS J1450+3908	41	14:50:30.65	+39:08:19.1	0.289	0.861	3.4	5.4	[5]
SDSS J1511+4713	24	15:11:18.74	+47:13:40.3	0.452	0.980	4.4	4.4	[7]
SDSS J1527+0652	39	15:27:45.02	+06:52:33.9	0.390	2.759	...	...	[12]
SDSS J1629+3528	27	16:29:54.56	+35:28:39.5	0.170	0.850	3.6	4.1	[7]
SDSS J1723+3411	14	17:23:36.16	+34:11:58.1	0.444	0.995	...	...	[18]
SDSS J1958+5950	128	19:58:35.32	+02:57:30.2	0.214	2.225	6.2	9.3	This paper
SDSS J2158+0257	163	21:58:43.68	+02:57:30.2	0.285	2.081	3.5	6.5	This paper
SDSS J2222+2745	159	22:22:08.68	+27:45:35.6	0.485	2.309, 2.807	8.0	6.2	[16], This paper
SDSS J2238+1319	10	22:38:31.31	+13:19:55.9	0.413	0.724	...	...	[13]
SDSS J2300+2213	111	23:00:17.25	+22:13:29.7	0.443	1.93	...	...	This paper

Table 4. Lens models of the full CASSOWARY spectroscopic sample. Systems for which the existing data do not allow a reliable model are listed in the table, but no model details are provided. References.– [1] Allam et al. 2007; [2] Shin et al. 2008; [3] Diehl et al. 2009; [4] Hainline et al. 2009; [5] Kubo et al. 2011; [6] Belokurov et al. 2009; [7] Kubo et al. 2009; [8] Sand et al. 2005; [9] Belokurov et al. 2007; [10] Lin et al. 2008; [11] Ofek et al. 2008; [12] Koester et al. 2010; [13] Bayliss et al. 2011; [14] Christensen et al. 2010; [15] Pettini et al. 2009; [16] Dahle et al. 2012; [17] Jones et al. (2013), [18] CASSOWARY data release; [19] Wuyts et al. 2012.

in Table 1. The flux ratio of Hα and Hβ (2.79) suggest that the nebular gas is largely unattenuated by dust, while the rest-frame EW of Hα emission ($\gtrsim 300$ Å) points to ionising radiation from a reasonably young ($\lesssim 100$ Myr for constant star formation history using nebular emission models described in Robertson et al. 2010) stellar population. The detection of [OIII] λ4363 (Figure 3) enables a measurement of the electron temperature ($T_e \simeq 1.5\times10^4$ K) which can be used along with the measured line ratios of the oxygen lines (following Izotov et al. 2006) to compute the oxygen abundance of the gas. Not surprisingly given the young age and lack of dust,

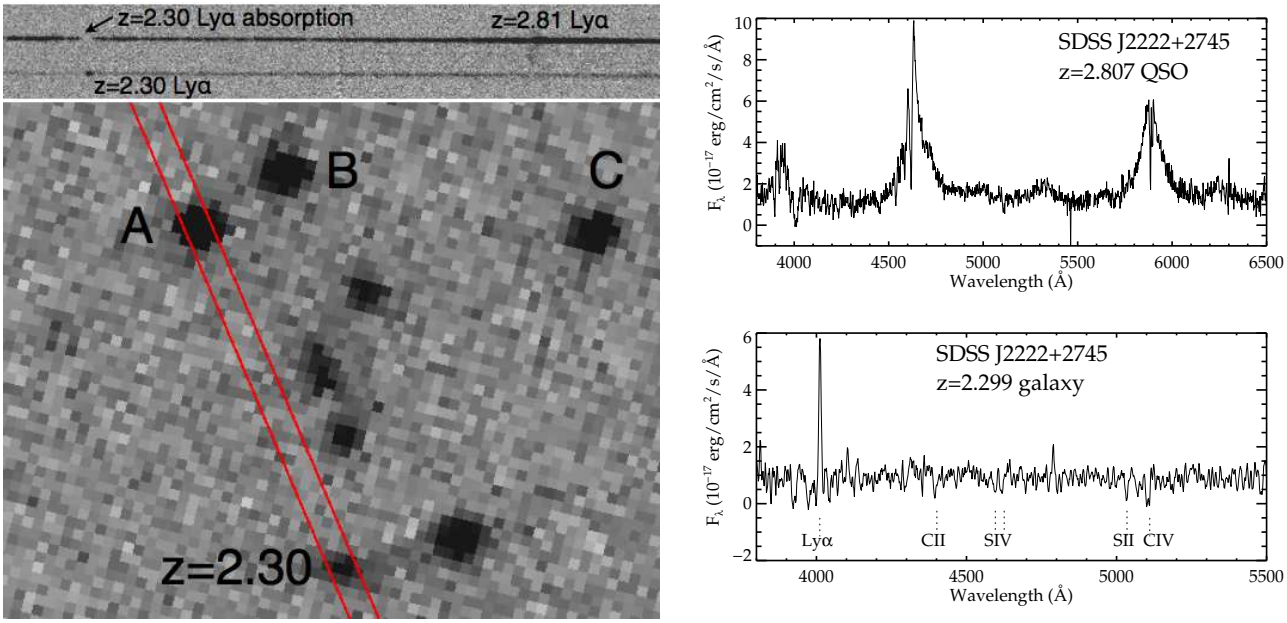

Figure 5. The bright lensed $z = 2.807$ quasar images in SDSSJ2222+2745 enable the opportunity to characterise the kinematics and metal content of the gas within $\simeq 50$ kpc of a bright lensed $z = 2.299$ galaxy. (*Left:*) The SDSS g-band image (bottom panel) clearly shows three of the six known images of the $z = 2.807$ quasar (which we labeled as A, B, and C) and a $z = 2.299$ lensed galaxy. We have obtained three separate MMT spectra of this system, one of which is denoted by the red lines. A portion of one of the 2D MMT spectrum is shown at top. Clearly visible is Lyα emission from the galaxy (bottom spectrum) and extended Lyα emission from the quasar (top). Notice the complete absorption of the quasar continuum at the observed wavelength corresponding to Lyα in the frame of the $z = 2.299$ galaxy. (*Right:*) Extracted MMT spectra of quasar image A (top) and lensed galaxy (bottom). Absorption of the quasar continuum near 4010 Å indicates the presence of neutral hydrogen at an impact parameter of roughly $\simeq 50$ kpc from the $z = 2.299$ galaxy.

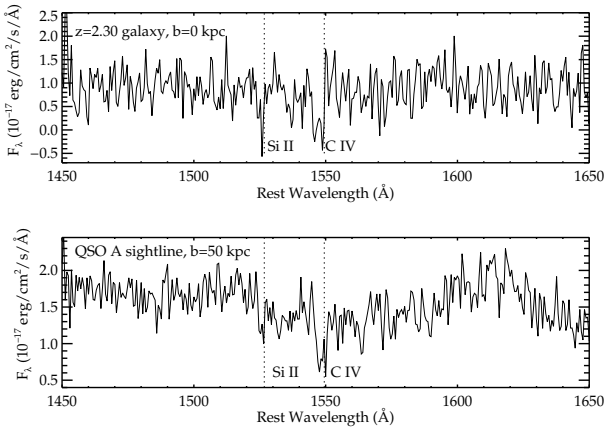

Figure 6. Spectra illustrating spatial extent of Si II and CIV gas associated with lensed $z = 2.299$ galaxy in SDSS J2222+2745. (*Top:*) Si II λ1526 and CIVλ1549 absorption along the line of sight toward the $z = 2.299$ galaxy. (*Bottom:*) Spectrum of the $z = 2.807$ quasar shifted to the rest-frame of the $z = 2.299$ galaxy. The quasar continuum shows absorption from Si II λ1526 and CIV λ1549, highlighting the presence of metals at an impact of ~ 50 kpc.

SDSS J0846+9446 appears to be one of the more metal poor galaxies known at high redshift with 12+log(O/H)$\simeq 8.0$ (~ 0.2 Z$_\odot$).

The lower limit we place on the [OIII] λ5007 rest-frame EW (>320 Å) is in the range spanned by the population of extreme line emitting galaxies (EELGs) identified in imaging and grism surveys (e.g., Kakazu et al. 2007; Hu et al. 2009; Atek et al. 2010 ; van der Wel et al. 2012). The number density of EELGs at $z \simeq 1.5 - 2$ is large enough to indicate that they are likely an important mode of star formation among low mass galaxies at high redshift and may well represent the manner in which the stellar mass in dwarf galaxies is assembled (e.g., van der Wel et. 2012). Yet as a result of their faint continuum flux densities, our understanding of the detailed properties of extreme line emitters at $z > 1$ remains limited (see Hu et al. 2009 for a detailed discussion at $z \simeq 0 - 1$).

By finding a highly-magnified example of such a system, we can begin to study this population in far more detail than would be possible in unlensed examples at $z \simeq 1.5 - 2.0$. With the spectra we have acquired to date for SDSS J0846+9446, we will be able to explore the relative chemical abundances in the ionised gas and to characterise the properties of the outflowing gas and stellar populations. Such an in depth analysis is beyond the scope of the present catalog paper and will appear in a separate work.

5.2 Spatial extent of gas around a $z = 2.3$ galaxy

The rest-UV absorption line spectra presented in Figure 2 provide information on the kinematics and chemical content of outflowing gas in galaxies at high redshift but do not reveal the exact location of the gas along the line of sight. Without knowledge of the spatial extent of the outflowing material, it is virtually impossible to characterise the energetics associated with the outflows. Spectra of bright background galaxies or quasars near the line of sight of a given galaxy provide a means of overcoming this shortcoming.

Steidel et al. (2010) conducted a comprehensive analysis of composite spectra of galaxy pairs, providing constraints on the distribution and covering fraction of circumgalactic gas on physical scales spanning 3-125 kpc. The stacked spectra revealed metal line

absorption at distances of $\simeq 60$ kpc and Lyα absorption from neutral hydrogen on physical scales in excess of 100 kpc.

A logical goal for the future is to extend constants on the spatial extent of outflows to individual systems. Most unlensed galaxy pairs are much too faint for useful constraints on the spatial extent of outflows. Steidel et al. (2010) present a case study for one of the brightest pairs in their sample, revealing CIV and Al II absorbing gas at an impact parameter of 16 kpc from a $z = 1.61$ galaxy. The continuum magnitudes of this particularly pair (g'=23.5 and 23.7) are $\simeq 1$ magnitude brighter than typical galaxies in their sample, making this a unique measurement at $z \simeq 2$.

Lensing clusters offer a feasible way of constraining the spatial distribution of circumgalactic gas on a source by source basis. The cluster environment offers two advantages. First the surface density of background sources is enhanced, providing more probes of the spatial distribution of gas associated with any individual lensed galaxy. Second, the flux magnification provided to lensed systems enables much higher S/N (and higher resolution) spectra to be obtained. With constraints from multiple impact parameters per galaxy (at various position angles), it should be possible to characterise the spatial and angular distribution of circumgalactic gas associated with an individual lensed galaxy. But with these advantages also comes difficulty, as knowledge of the impact parameters of the lensed background galaxies can only be obtained with a reliable cluster mass model, limiting analysis to well-constrained lenses.

The close proximity of a bright ($g \simeq 21$ as measured in deeper imaging presented in Dahle et al. 2012) lensed $z = 2.30$ galaxy to three bright images of a lensed $z = 2.81$ quasar in SDSS J2222+2745 (Figure 4) enables immediate constraints on the circumgalactic gas associated with the foreground $z = 2.30$ galaxy. The brightest quasar images are separated by 14, 15, and 16 arc seconds with respect to the galaxy. But the relevant quantity for calculating the impact parameter is of course the separation in the source plane of the $z = 2.30$ galaxy. Using our lens model for this cluster (see §4.2), we find that the quasar absorption line spectra probes gas associated with the $z = 2.30$ galaxy on physical scales of 50 kpc. While each quasar image probes the same impact parameter, the individual spectra can be stacked allowing fainter absorption features to be detected.

The relatively shallow spectra we have obtained with MMT provide a first glimpse of the spatial extent of circumgalactic gas around the lensed $z = 2.30$ galaxy. It is immediately apparent in the 2D spectrum that the quasar continuum in image A is completely extinguished at the wavelength corresponding to Lyα in the rest-frame of the $z = 2.30$ galaxy. The centroid of the $z = 2.30$ Lyα absorption in the quasar spectrum occurs at roughly 4010 Å with strong absorption spanning $\sim$ 4000-4020 Å. This is not surprisingly somewhat bluer than the wavelength of the Lyα emission(4012 Å) in the galaxy spectrum. Metal absorption from the CGM of the $z = 2.30$ galaxy is also apparent in quasar spectrum. We clearly detect CIV absorption at ~ 5110 Å and tentatively identify absorption from Si II λ1526 at 5034 Å in the quasar spectrum (Figure 5). Higher S/N and higher resolution observations are required to characterise the profiles of the absorption lines in both the quasar and galaxy.

Deeper spectra of the quasar images should reveal the presence of other ions associated with the $z = 2.3$ galaxy at the 50 kpc impact parameter, providing a more detailed picture of the chemical makeup and ionisation state of material associated with the galaxy. Meanwhile as deeper multi-wavelength images of the field around SDSSJ2222+2745 emerge, it should be possible to identify additional lensed systems behind the $z = 2.30$ galaxy. Spectra of these systems should yield a map of the spatial and angular distribution of outflowing gas associated with this galaxy.

5.3 Intervening absorption from foreground lens

Deep spectra of the background lensed galaxies can also provide information on the CGM of the quiescent central lens galaxy. In particular, if a significant component of cool gas resides in the halos of the early-type lens galaxies (as expected from the QSO absorption line results presented in Werk et al. 2012), then we should detect absorption from Mg II or Fe II transitions in the spectra of the background source. Given the range of angular separations between arcs and lenses, the background lensed galaxies probe impact parameters of $\simeq 20 - 60$ kpc.

To detect metal line absorption in the background lensed source requires that the lens be at high enough redshift to place either Mg II or Fe II transitions in the optical window. This limits the test to lenses at $z \gtrsim 0.35$ (for Mg II) and $z \gtrsim 0.45$ (for Fe II λ2600). As is clear from Table 4, many of the CASSOWARY systems satisfy these criteria.

We have examined the MMT source spectra for possible signs of absorption from cool gas associated with the lens. As noted in §3.2, there are two cases in which we suggest that intervening absorption might be associated with the lens. In SDSS J0145-0455 (Figure 2), the absorption feature at 4244 Å might correspond to Fe II λ2600 absorption from the central lens. We should be able to confirm this identification through detection of Mg II absorption, but given the limited resolution of the MMT spectra, Mg II absorption at the lens redshift is blended with the broad CIV absorption from the background arc. A higher resolution spectrum is needed to confirm the nature of the absorption system. In the arc toward SDSS J1439+3250, we detect absorption at 3970 Å, which may stem from Mg II at the redshift ($z = 0.418$) of the lens. This identification is complicated by the fact that we have not yet confirmed the redshift of the arc, making it impossible at this stage to disentangle whether a given absorption feature stems from the arc or lens. Several other systems with MMT spectra show hints of absorption at the wavelength expected for Mg II, but as a result of our limited S/N and low spectral resolution, it is not yet possible to make definitive identifications.

As higher S/N and higher resolution spectra of the lensed galaxies emerge, it should become feasible to put constraints on the properties of cool gas associated with quiescent galaxies at $z \simeq 0.4-0.7$. In the ideal scenario in which the background source forms a complete Einstein ring, such absorption line studies offer the potential to create a full two-dimensional map (at a single impact parameter) of the CGM of the lens, complementing ongoing work with quasar absorption lines (e.g., Chen et al. 2010; Werk et al. 2012).

6 SUMMARY

The discovery of bright gravitationally-lensed galaxies has begun to make a significant impact on our understanding of star formation and feedback at high redshift. Once a field focused on the few bright highly-magnified galaxies known (e.g., Pettini et al. 2001), sky surveys like SDSS and targeted HST imaging of massive clusters have opened the door for the construction of much larger samples of bright lensed galaxies. For several years, our

team (CASSOWARY) has been identifying galaxy-galaxy lens candidates within the SDSS imaging data (e.g., Belokurov et al. 2007, 2009). Yet the impact of detailed follow-up efforts has been stunted by the low percentage of the brightest lensed systems with confirmed redshifts.

In this paper, we present the results of a spectroscopic campaign aimed at confirming the redshifts of a larger fraction of the CASSOWARY lensed candidates identified in SDSS. Our ultimate goal is to increase the number of suitable targets for resolved IFU infrared spectroscopy (e.g., Stark et al. 2008; Jones et al. 2012b) and high resolution optical spectroscopy (Quider et al. 2009; 2010).

The spectroscopic data used to confirm redshifts in this paper were primarily obtained using the Blue and Red Channel Spectrographs on MMT, but we also observed select objects with spectrographs on Keck, LBT, and Magellan. Through these efforts, we have confirmed the redshifts of 25 bright lensed objects (24 galaxies and 1 quasar) in SDSS. Only two of the lensed systems (the galaxy and quasar behind SDSS 2222+2745 and the $z = 0.909$ galaxy toward SDSS J1138+2754) have been presented with redshifts (Dahle et al. 2012; Wuyts et al. 2012). The new redshift sample contains two of the brightest ($r \lesssim 20$) high redshift galaxies known in SDSS, a young, metal poor (0.2 $Z_{\odot}$) extreme line emitting star forming system at $z = 1.43$, and many further systems which are bright enough for detailed studies. We provide a brief discussion of the spectroscopic properties of each system, focusing on the absorption or emission features used for redshift confirmation.

With the new redshift catalog presented in this paper, the total number of spectroscopically-confirmed lensed systems in the CASSOWARY SDSS database now stands at 55. Our initial attempts at lens modelling of the CASSOWARY systems suggests that source magnification factors are typically in the range of 5-10×. Given the range of SDSS apparent magnitudes of the sources, we crudely estimate typical star formation rates (20-100 $M_{\odot}$ yr^{-1}) and stellar masses (10^{10} - 10^{11} $M_{\odot}$) of the $z \simeq 2$ lensed population. Deeper imaging will be required to extend these estimates robustly to individual systems. Detailed spectroscopic follow-up of these systems is underway and will be presented in future papers. With 26 bright lensed systems in the CASSOWARY catalog at $z \gtrsim 1.8$ and a further 10 at $1.3 \lesssim z \lesssim 1.8$, it will soon be possible to infer more generalised conclusions from detailed spectroscopic study of the brightest lensed galaxies.

ACKNOWLEDGMENTS

We thank Fuyan Bian, Zheng Cai, Linhua Jiang, Ian McGreer, and Evan Schneider for conducting some of the observations used in this paper. DPS acknowledges support from NASA through Hubble Fellowship grant #HST-HF-51299.01 awarded by the Space Telescope Science Institute, which is operated by the Association of Universities for Research in Astronomy, Inc, for NASA under contract NAS5-265555. BER is supported by Steward Observatory and the University of Arizona College of Science. Observations reported here were obtained at the MMT Observatory, a joint facility of the University of Arizona and the Smithsonian Institution.

REFERENCES

Allam, S. S., Tucker, D. L., Lin, H., et al. 2007, ApJL, 662, L51
Atek, H., Siana, B., Scarlata, C., et al. 2011, ApJ, 743, 121
Auger, M. W., Treu, T., Brewer, B. J., & Marshall, P. J. 2011, MNRAS, 411, L6
Bayliss, M. B., Gladders, M. D., Oguri, M., et al. 2011a, ApJL, 727, L26
Bayliss, M. B., Hennawi, J. F., Gladders, M. D., et al. 2011b, ApJS, 193, 8
Bayliss, M. B. 2012, ApJ, 744, 156
Belokurov, V., Evans, N. W., Moiseev, A., et al. 2007, ApJL, 671, L9
Belokurov, V., Evans, N. W., Hewett, P. C., et al. 2009, MNRAS, 392, 104
Bian, F., Fan, X., Bechtold, J., et al. 2010, ApJ, 725, 1877
Bouwens, R. J., Illingworth, G. D., Franx, M., et al. 2009, ApJ, 705, 936
Brammer, G. B., Sánchez-Janssen, R., Labbé, I., et al. 2012, ApJL, 758, L17
Brewer, B. J., Lewis, G. F., Belokurov, V., et al. 2011, MNRAS, 412, 2521
Chen, H.-W., Wild, V., Tinker, J. L., et al. 2010, ApJL, 724, L176
Christensen, L., D'Odorico, S., Pettini, M., et al. 2010, MNRAS, 406, 2616
Christensen, L., Richard, J., Hjorth, J., et al. 2012, MNRAS, 427, 1953
Christensen, L., Laursen, P., Richard, J., et al. 2012, MNRAS, 427, 1973
Dahle, H., Gladders, M. D., Sharon, K., et al. 2012, arXiv:1211.1091
Diehl, H. T., Allam, S. S., Annis, J., et al. 2009, ApJ, 707, 686
Dye, S., Evans, N. W., Belokurov, V., Warren, S. J., & Hewett, P. 2008, MNRAS, 388, 384
Ebeling, H., Edge, A. C., Mantz, A., et al. 2010, MNRAS, 407, 83
Eisenstein, D. J., Annis, J., Gunn, J. E., et al. 2001, AJ, 122, 2267
Erb, D. K., Quider, A. M., Henry, A. L., & Martin, C. L. 2012, ApJ, 759, 26
Faber, S. M., Phillips, A. C., Kibrick, R. I., et al. 2003, Proc. SPIE , 4841, 1657
Fosbury, R. A. E., Villar-Martín, M., Humphrey, A., et al. 2003, ApJ, 596, 797
Genzel, R., Newman, S., Jones, T., et al. 2011, ApJ, 733, 101
Hainline, K. N., Shapley, A. E., Kornei, K. A., et al. 2009, ApJ, 701, 52
Hennawi, J. F., Gladders, M. D., Oguri, M., et al. 2008, AJ, 135, 664
Hu, E. M., Cowie, L. L., Kakazu, Y., & Barger, A. J. 2009, ApJ, 698, 2014
Izotov, Y. I., Stasińska, G., Meynet, G., Guseva, N. G., & Thuan, T. X. 2006, A&A, 448, 955
Jones, T. A., Swinbank, A. M., Ellis, R. S., Richard, J., & Stark, D. P. 2010a, MNRAS, 404, 1247
Jones, T., Ellis, R., Jullo, E., & Richard, J. 2010b, ApJL, 725, L176
Jones, T., Stark, D. P., & Ellis, R. S. 2012a, ApJ, 751, 51
Jones, T., Ellis, R. S., Richard, J., & Jullo, E. 2012b, arXiv:1207.4489
Kakazu, Y., Cowie, L. L., & Hu, E. M. 2007, ApJ, 668, 853
Koester, B. P., Gladders, M. D., Hennawi, J. F., et al. 2010, ApJL, 723, L73
Kormann, R., Schneider, P., & Bartelmann, M. 1994, A&A, 284, 285
Kornei, K. A., Shapley, A. E., Martin, C. L., et al. 2012, ApJ, 758, 135
Kubo, J. M., Allam, S. S., Annis, J., et al. 2009, ApJL, 696, L61
Kubo, J. M., Allam, S. S., Drabek, E., et al. 2010, ApJL, 724, L137
Lin, H., Buckley-Geer, E., Allam, S. S., et al. 2009, ApJ, 699, 1242
Martin, C. L., Shapley, A. E., Coil, A. L., et al. 2012, ApJ, 760, 127
Newman, S. F., Genzel, R., Förster-Schreiber, N. M., et al. 2012, ApJ, 761, 43
Ofek, E. O., Seitz, S., & Klein, F. 2008, MNRAS, 389, 311
Pettini, M., Steidel, C. C., Adelberger, K. L., Dickinson, M., & Giavalisco, M. 2000, ApJ, 528, 96
Pettini, M., Rix, S. A., Steidel, C. C., et al. 2002, ApJ, 569, 742
Pettini, M., Chritensen, L., D'Odorico, S., et al. 2010, MNRAS, 402, 2335
Quider, A. M., Pettini, M., Shapley, A. E., & Steidel, C. C. 2009, MNRAS, 398, 1263
Quider, A. M., Shapley, A. E., Pettini, M., Steidel, C. C., & Stark, D. P. 2010, MNRAS, 402, 1467
Reddy, N. A., Erb, D. K., Pettini, M., Steidel, C. C., & Shapley, A. E. 2010, ApJ, 712, 1070
Reddy, N., Dickinson, M., Elbaz, D., et al. 2012a, ApJ, 744, 154
Reddy, N. A., Pettini, M., Steidel, C. C., et al. 2012b, ApJ, 754, 25
Richard, J., Jones, T., Ellis, R., et al. 2011, MNRAS, 413, 643
Rigby, J. R., Wuyts, E., Gladders, M. D., Sharon, K., & Becker, G. D. 2011, ApJ, 732, 59

Robertson, B. E., Ellis, R. S., Dunlop, J. S., McLure, R. J., & Stark, D. P. 2010, Nature, 468, 49
Sand, D. J., Treu, T., Ellis, R. S., & Smith, G. P. 2005, ApJ, 627, 32
Shapley, A. E., Steidel, C. C., Pettini, M., & Adelberger, K. L. 2003, ApJ, 588, 65
Shin, M.-S., Strauss, M. A., Oguri, M., et al. 2008, AJ, 136, 44
Simcoe, R. A., Burgasser, A. J., Bochanski, J. J., et al. 2010, Proc. SPIE , 7735,
Stark, D. P., Swinbank, A. M., Ellis, R. S., et al. 2008, Nature, 455, 775
Steidel, C. C., Erb, D. K., Shapley, A. E., et al. 2010, ApJ, 717, 289
Swinbank, A. M., Webb, T. M., Richard, J., et al. 2009, MNRAS, 400, 1121
van der Wel, A., Straughn, A. N., Rix, H.-W., et al. 2011, ApJ, 742, 111
Weiner, B. J., Coil, A. L., Prochaska, J. X., et al. 2009, ApJ, 692, 187
Wen, Z.-L., Han, J.-L., & Jiang, Y.-Y. 2011, Research in Astronomy and Astrophysics, 11, 1185
Werk, J. K., Prochaska, J. X., Thom, C., et al. 2013, ApJS, 204, 17
Wuyts, E., Rigby, J. R., Sharon, K., & Gladders, M. D. 2012, ApJ, 755, 73
Yuan, T.-T., & Kewley, L. J. 2009, ApJL, 699, L161
Yuan, T.-T., Kewley, L. J., Swinbank, A. M., Richard, J., & Livermore, R. C. 2011, ApJL, 732, L14
Yuan, T.-T., Kewley, L. J., & Richard, J. 2013, ApJ, 763, 9